

Topological Magnetic Excitations on the Distorted Kagomé Antiferromagnets: Applications to Volborthite, Vesignieite, and Edwardsite.

S. A. Owerre^{1,2}

¹*Perimeter Institute for Theoretical Physics, 31 Caroline St. N., Waterloo, Ontario N2L 2Y5, Canada.*

²*African Institute for Mathematical Sciences, 6 Melrose Road, Muizenberg, Cape Town 7945, South Africa.*

Inelastic neutron scattering experiment has uncovered a finite thermal Hall conductivity on the frustrated distorted kagomé volborthite at nonzero magnetic field with no signal of Dzyaloshinskii-Moriya (DM) spin-orbit interaction. The observed thermal Hall response is attributed to an emergence of nontrivial elementary excitations in the quantum spin liquid phase. However, the origin of the nontrivial topological magnetic excitations and the associated thermal Hall response has not been identified unlike in collinear unfrustrated magnets where it is well established that the DM interaction is the driving force. Several distorted kagomé antiferromagnets, such as vesignieite, edwardsite, and volborthite show evidence of magnetic long-range order at low temperatures. Here, we identify a chiral noncoplanar spin order on the distorted kagomé-lattice antiferromagnets induced by the presence of a magnetic field applied perpendicular to the distorted kagomé plane. The noncoplanar spin texture has a nonzero scalar spin chirality similar to a chiral quantum spin liquid with broken time-reversal symmetry. In the noncoplanar regime, the DM interaction is immaterial and nontrivial topological magnetic excitations manifest through field-induced scalar spin chirality. The associated Hall response is termed “topological” thermal Hall effect as it originates from the real space Berry curvature of the spin texture rather than the DM spin-orbit interaction.

I. INTRODUCTION

A chiral spin liquid (CSL) is a particular type of spin liquids in which time-reversal symmetry (TRS) is broken macroscopically [1–3]. The scalar spin chirality $\langle \chi_{ijk} \rangle = \langle \mathbf{S}_i \cdot (\mathbf{S}_j \times \mathbf{S}_k) \rangle$ defines the hallmark of a CSL. It is also generally believed that the magnetic excitations in any quantum spin liquid (QSL) are bosonic spin-1/2 spinons in which the conventional bosonic spin-1 magnons fractionalize. According to Kalmeyer and Laughlin [1] a CSL can be thought of as a bosonic version of $\nu = 1/2$ Laughlin state in fractional quantum Hall effect. In recent years, a plethora of theoretical models has been proposed in which a CSL phase can be stabilized. The recent theoretical numerical work shows that a CSL can emerge in a kagomé lattice Mott insulator in which a magnetic field induces an explicit spin chirality interaction in a t/U perturbative expansion of the Hubbard model at half filling [4], hence TRS is broken explicitly. In other numerical works a spontaneously broken TRS CSL is found away from the isotropic kagomé-lattice antiferromagnet by adding additional second and third nearest neighbour interactions [5–9] or Ising anisotropy [10].

In real materials, however, a CSL has remained elusive because material synthesis usually comes with defects such as structural distortion and perturbative anisotropy like the intrinsic DM spin-orbit interaction [11, 12], which tend to destabilize disordered QSL and induce a magnetic long-range order. For quantum kagomé antiferromagnets (QKAF), various experimentally accessible materials such as iron jarosites [13–16], vesignieite $\text{BaCu}_3\text{V}_2\text{O}_8(\text{OH})_2$ [17–23], edwardsite $\text{Cd}_2\text{Cu}_3(\text{SO}_4)_2(\text{OH})_6 \cdot 4\text{H}_2\text{O}$ [24], and volborthite $\text{Cu}_3\text{V}_2\text{O}_7(\text{OH})_2 \cdot 2\text{H}_2\text{O}$ [25–28] have long-range magnetic orders below certain temperatures and they are generally attributed to the presence of DM spin-orbit inter-

action. The recent proposals of QSL materials are herbertsmithite $\text{ZnCu}_3(\text{OH})_6\text{Cl}_2$ [29, 30] and the calcium-chromium oxide $\text{Ca}_{10}\text{Cr}_7\text{O}_{28}$ [31] which show a continuum of spinon excitations in inelastic neutron scattering experiment [31, 32]. Nevertheless, an applied magnetic field or pressure destabilizes the QSL nature of these materials and leads to field-induced magnetic order at low temperatures [31, 33, 34].

The emerging experimental technique to probe the nature of magnetic excitations in QSL materials is the measurement of thermal Hall effect of charge-neutral magnetic spin excitations. For ordered quantum magnets thermal Hall effect has been realized in the collinear kagomé ferromagnet $\text{Cu}(1-3, \text{bdc})$ [35] and a number of collinear pyrochlore ferromagnets [36, 37]. In this case the transverse thermal Hall conductivity (κ_{xy}) can be explained in terms of Berry curvature induced by the DM spin-orbit interaction [38–40] leading to topological magnons [41–49] and Weyl magnons [50, 51] similar to spin-orbit coupling electronic systems [52–56]. In a recent experiment [57], a nonzero κ_{xy} has been observed in a frustrated distorted kagomé volborthite, at a strong magnetic field of 15 T with no signs of the DM spin-orbit interaction and no discernible thermal Hall signal was observed at zero magnetic field [58]. The authors attributed the presence of κ_{xy} to nontrivial elementary excitations in the gapless QSL phase, however a strong field of 15 T causes low-temperature magnetic phases in volborthite [26–28]. Nevertheless, the exact nature of the magnetic phases at 15 T is poorly understood, but the intrinsic DM spin-orbit anisotropy suggests a $\mathbf{Q} = \mathbf{0}$ coplanar/noncollinear Néel order.

Exact diagonalization study has established a quantum critical point (QCP) induced by the out-of-plane DM spin-orbit anisotropy in spin-1/2 QKAF given by $D_{\perp}^c/J \sim 0.1$ [59]. A moment free QSL phase is pre-

II. MODEL

The exact spin Hamiltonian that describes kagomé volborthite has been very controversial. Attempts to describe previous experimental features of volborthite have led to different proposals of spin Hamiltonian which include: coupled frustrated chains [60, 61], coupled trimers [62], and anisotropic Heisenberg exchange model [63–67]. In this paper, we will adopt the latter model. We consider the microscopic spin Hamiltonian on the distorted QKAF subject to a magnetic field perpendicular to the kagomé plane. The Hamiltonian is given by

$$\mathcal{H} = \sum_{nn} [J_{ij} \mathbf{S}_i \cdot \mathbf{S}_j + \mathbf{D}_{ij} \cdot \mathbf{S}_i \times \mathbf{S}_j] - \mathbf{H} \cdot \sum_i \mathbf{S}_i, \quad (1)$$

where \mathbf{S}_i is the magnetic spin moment at site i , $J_{ij} = J > 0$ on the diagonal bonds and $J_{ij} = J' = J\delta$ on the horizontal bonds with $\delta \neq 1$ as shown in Fig. 1. The inversion symmetry breaking on the kagomé lattice allows a DM vector $\mathbf{D}_{ij} = -D_\perp \hat{\mathbf{z}}$ and they lie at the midpoints between two magnetic ions as shown in Fig. 1. The last term is the out-of-plane external magnetic field $\mathbf{H} = h\hat{\mathbf{z}}$ and $h = g\mu_B H$. The out-of-plane DM interaction stabilizes the coplanar/noncollinear spin configuration [13]. In some kagomé materials an in-plane DM interaction D_\parallel may be present due to lack of mirror planes. It leads to weak out-of-plane ferromagnetism with small ferromagnetic moment. However, it is usually negligible compared to the out-of-plane component for most spin-1/2 kagomé antiferromagnetic materials [30, 59] and can be removed by gauge transformation. For kagomé volborthite [57], there was no signal of both in-plane and out-of-plane DM interaction on the observed κ_{xy} . Also, for potassium Fe-jarosite with spin-5/2 the in-plane DM interaction (or the DM interaction in general) does not necessarily induce topological magnetic excitations [16]. Therefore, we will neglect the small in-plane DM component at the moment and comment on its effects in the subsequent sections.

Let us start from what is known for distorted kagomé antiferromagnets at $\mathbf{D}_{ij} = h = 0$ [65]. In this case, the Hamiltonian can be written as

$$\mathcal{H} = \frac{J\delta}{2} \sum_{\Delta} \left(\frac{1}{\delta} \mathbf{S}_A + \mathbf{S}_B + \mathbf{S}_C \right)^2 - \text{const.}, \quad (2)$$

where $\mathbf{S}_{A,B,C}$ form a triad as depicted in Fig. 1. It is easily seen that the classical energy is minimized for $\frac{1}{\delta} \mathbf{S}_A + \mathbf{S}_B + \mathbf{S}_C = 0$, yielding $\vartheta = \arccos(-1/2\delta) \neq 120^\circ$ for $\delta \neq 1$. The classical configuration is now a canted coplanar/noncollinear spins for $\delta > 1/2$ [65]. However, it also has an extensive degeneracy as in the ideal kagomé Heisenberg antiferromagnets. There are several limiting cases in which the system is either bipartite with collinear magnetic order or non-bipartite with non-collinear magnetic order. The limiting case $\delta \rightarrow 0$ maps to a bipartite square lattice with collinear magnetic order and $\delta \rightarrow \infty$ maps to a decoupled antiferromagnetic chains.

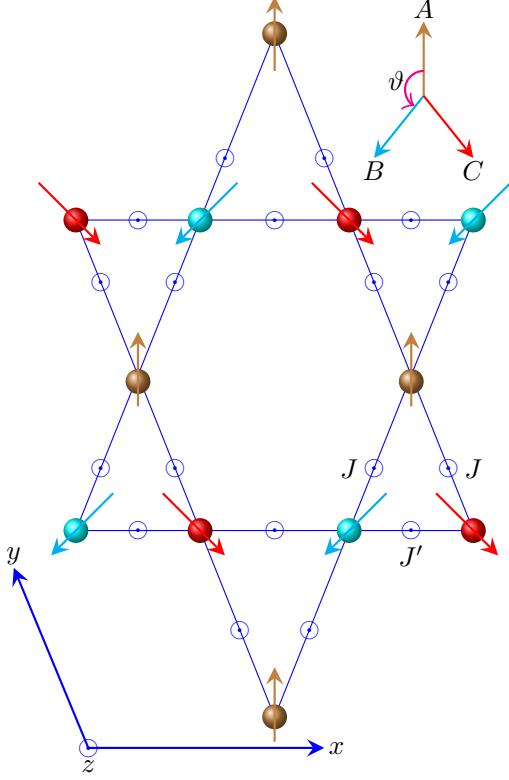


FIG. 1. Color online. Canted coplanar/noncollinear magnetic order on the distorted kagomé lattice with positive vector chirality. The out-of-plane DM interaction lies at the midpoints between two magnetic ions as indicated by small dotted circles. The spin triad are separated by an angle $\vartheta \neq 120^\circ$ on each isosceles triangle with $J \neq J'$ as shown at the top figure.

dicted for $D_\perp/J < D_\perp^c/J$ and a $\mathbf{Q} = \mathbf{0}$ Néel phase exists for $D_\perp/J > D_\perp^c/J$. From different experimental inspections, it is generally believed that both edwardsite and vesignieite are located in the ordered regime below certain temperature with $0.1 < D_\perp/J < 0.16$ [19, 20], as well as volborthite. But herbertsmithite $\text{ZnCu}_3(\text{OH})_6\text{Cl}_2$ has $D_\perp/J \sim 0.08$ [30], thus remain a QSL. In both the Néel phase and the QSL phase an applied magnetic field ($\mathbf{H} \perp 2\text{D plane}$) can induce noncoplanar spin textures with a nonzero scalar spin chirality. The emergent scalar spin chirality due to noncoplanar spins might be different from the spontaneous scalar spin chirality in the CSL, but their effects on the magnetic excitations should be the same. In this paper we show that a nonzero Berry curvature can be induced by the spin texture in real space rather than the DM spin-orbit interaction. The Berry curvature stems from the emergent scalar spin chirality which measures the solid angle subtended by three spins in a unit triangular plaquette of the kagomé lattice. The real space Berry curvature drives the thermal Hall effect in frustrated QKAF with/without magnetic long-range order.

For $\delta < 1/2$ it has been established that the classical ground state is collinear (up-down-down state) and there is no degeneracy except a global spin rotation about the z -axis, and for $\delta > 1/2$ the classical ground state is non-collinear but coplanar. The collinear phases are trivial. In the present study, we focus on the canted coplanar/noncollinear regime ($\delta > 1/2$) as the ground state properties of volborthite, vesignieite, and edwardsite are believed to live in this regime.

III. CLASSICAL GROUND STATE

Now, we consider the classical ground state of the full Hamiltonian (1). In the classical limit, the spin operators can be approximated as classical vectors, written as $\mathbf{S}_i = S\mathbf{n}_i$, where $\mathbf{n}_i = (\sin\phi \cos\theta_i, \sin\phi \sin\theta_i, \cos\phi)$ is a unit vector and θ_i labels the spin oriented angles on the spin triad and ϕ is the magnetic-field-induced canting angle. For $\delta > 1/2$ the ground state is the canted coplanar/noncollinear spin configuration in Fig. 1. The classical energy is given by

$$e_0(\phi) = 2J(2 + \delta) [(1 - \cos\vartheta) \cos^2\phi + \cos\vartheta] - 4D_\perp \sin^2\phi \sin\vartheta(1 - \cos\vartheta) - 3h \cos\phi, \quad (3)$$

where $e_0(\phi) = E(\phi)/NS^2$, and N is the number of sites per unit cell. The magnetic field is rescaled in unit of S . The minimization of $e_0(\phi)$ yields the magnetic-field-induced canting angle $\cos\phi = h/h_s$ where

$$h_s = \frac{(1 - \cos\vartheta)}{3} [4J(2 + \delta) + 8D_\perp \sin\vartheta]. \quad (4)$$

As can be seen from Eq. 3 the classical energy depends on the DM interaction as it contributes to the stability of the coplanar/noncollinear spin configuration. In collinear spin configurations, the DM interaction does not contribute to the classical energy, instead it provides TMDs, e.g. in kagomé ferromagnets [35–39, 41–46, 50, 51].

IV. TOPOLOGICAL MAGNETIC EXCITATIONS

The magnetic excitations of frustrated QKAF can be studied in different formalisms. In real materials the intrinsic DM spin-orbit interaction and an external applied magnetic field are very likely to induce a magnetic long-range order in frustrated QKAF [26–28, 33, 34]. Therefore, we use the Holstein-Primakoff (HP) transformation [68] valid in the low-temperature regime. In the Supplemental Material (SM), we have shown that a magnetic field ($H \perp 2D$ plane) can induce a chiral noncoplanar spin texture with an emergent scalar spin chirality

$$\mathcal{H}_\phi = J_\phi \sum_{i,j,k,\Delta} \chi_{ijk}, \quad (5)$$

where $J_\phi = \cos\phi \propto H$. As we previously mentioned, the scalar spin chirality breaks time-reversal (\mathcal{T}) symmetry

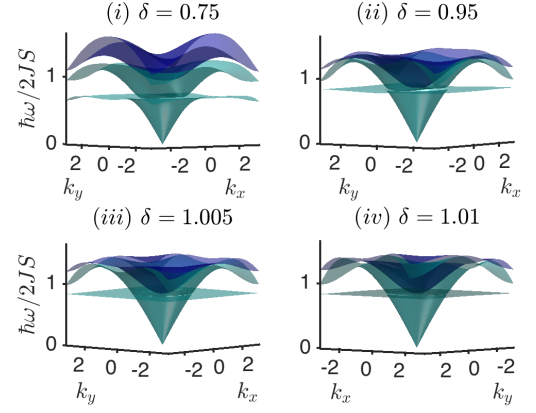


FIG. 2. Color online. Magnon dispersion of distorted kagomé antiferromagnet at zero magnetic field and several values of distortion with $D_\perp/J = 0.2$.

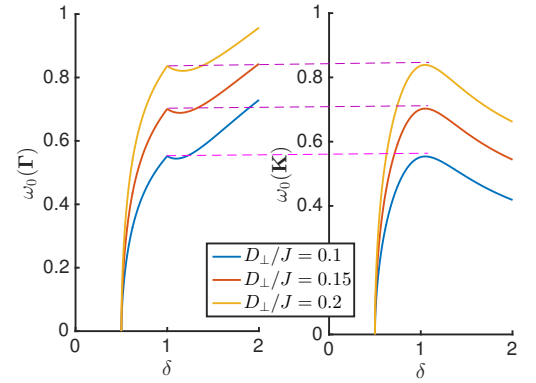


FIG. 3. Color online. The lifted zero mode ω_0 varies in the Brillouin zone as function of the distortion for zero magnetic field $\mathcal{H}_\phi = 0$. The dash lines connect isotropic point $\delta = 1$. The coplanar/noncollinear order is valid for $\delta > 0.5$.

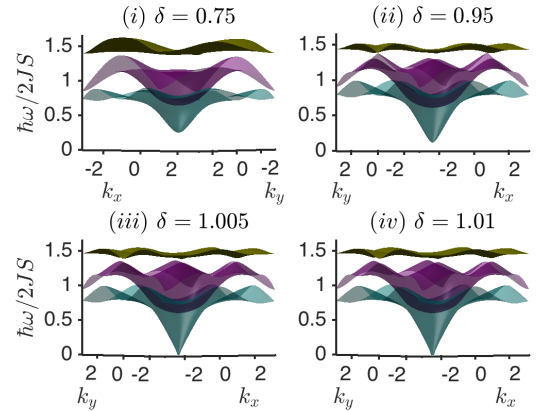


FIG. 4. Color online. Topological magnon dispersion of distorted kagomé antiferromagnet at finite magnetic-field-induced scalar spin chirality. The parameters chosen are $h/h_s = 0.3$ and $D_\perp/J = 0.2$.

macroscopically and can be spontaneously developed in CSL [1–8]. Its effects on the magnetic excitations should be the same in the ordered and disordered phases. In the magnetic-field-induced noncoplanar regime the DM interaction is immaterial, but the system still exhibits nontrivial topological effects through real space Berry curvature of the spin texture.

The magnetic excitations at zero magnetic field and zero DM interaction with $\delta \neq 1$ still exhibit a zero energy mode $\omega_0 = 0$ (not shown). Lattice distortion is unable to lift the zero energy mode. In addition, there are two non-degenerate dispersive modes $\omega_1 \neq \omega_2$ (not shown) induced by lattice distortion in contrast to undistorted kagomé antiferromagnets with degenerate modes $\omega_1 = \omega_2$. Although the exact parameter values of volborthite are not known, an out-of-plane DM interaction is intrinsic to the kagomé lattice. A moderate DM interaction ($D_\perp/J = 0.2$) lifts the zero energy mode and stabilizes the coplanar/noncollinear spin configuration as shown in Fig. 2. We find that the lifted zero mode is no longer a constant flat band but varies in the BZ (see SM), that is $\omega_0(\Gamma) \neq \omega_0(\mathbf{K})$, where $\Gamma = (0, 0)$ and $\mathbf{K} = (2\pi/3, 0)$ see Fig. 3. This is one of the differences between distorted and undistorted kagomé antiferromagnets at finite DM interaction. From symmetry point of view, the mirror reflection (\mathcal{M}) symmetry is a good symmetry of the kagomé lattice, but it reverses the in-plane spins in the x - y plane. Under \mathcal{T} -symmetry, the spins will be flipped again and return to the original state, hence \mathcal{TM} is a symmetry of the coplanar/noncollinear magnetic order. Since the lattice distortion and the out-of-plane DM interaction preserve this combined symmetry the system should be topologically trivial as we will show below. Therefore, we expect this model to be topologically nontrivial when either \mathcal{T} -symmetry or \mathcal{M} -symmetry is broken.

The combined symmetries can be broken in two ways. (i) If the kagomé lattice lacks \mathcal{M} -symmetry, an in-plane DM component D_\parallel might be present according to the Moriya rules [12]. The in-plane DM component preserves \mathcal{T} -symmetry but breaks \mathcal{M} -symmetry, hence \mathcal{TM} will be broken. This leads to weak out-of-plane ferromagnetism or noncoplanar spin canting with scalar spin chirality and weak ferromagnetic moment [13, 69]. Thus, for kagomé antiferromagnetic materials with $D_\perp \ll D_\parallel$ we expect the out-of-plane ferromagnetism to be dominant and hence the (in-plane) DM interaction should be the primary source of topological spin excitations as we already know in collinear ferromagnets with out-of-plane DM interaction. However, most kagomé antiferromagnetic materials have a dominant intrinsic out-of-plane component $D_\perp \gg D_\parallel$ and the weak ferromagnetism induced by D_\parallel can be negligible. In fact, there was no signal of any DM interaction on the observed κ_{xy} in kagomé volborthite [57]. Therefore, there must be another source of topological spin excitations apart from the DM interactions. (ii) An alternative way to break \mathcal{TM} symmetry is by applying an external magnetic field perpendicular to the kagomé plane ($\mathbf{H} \perp 2\text{D plane}$). A finite out-of-

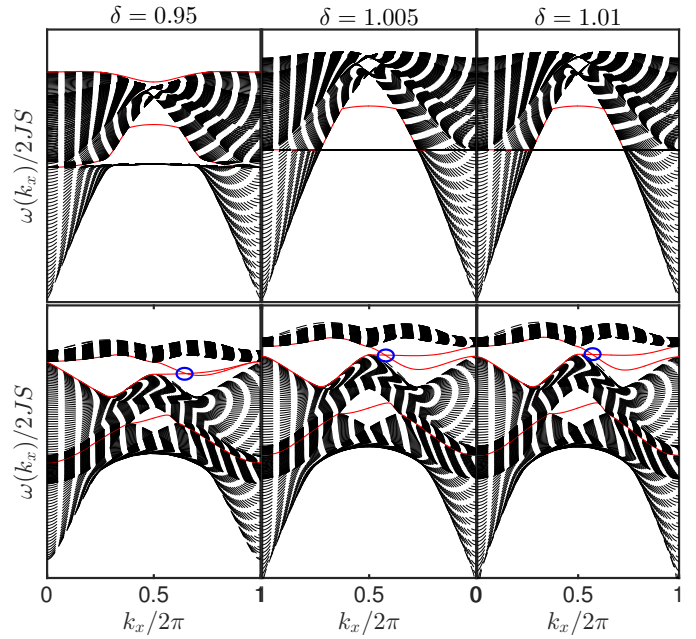


FIG. 5. Color online. Chiral magnon edge modes of distorted kagomé lattice for a strip geometry with $D_\perp/J = 0.2$. Top panel: $\mathcal{H}_\phi = 0$, $h/h_s = 0$. Bottom panel: $\mathcal{H}_\phi \neq 0$, $h/h_s = 0.3$.

plane magnetic field breaks \mathcal{T} -symmetry but preserves \mathcal{M} -symmetry. It induces a noncoplanar spin texture with a nonzero scalar spin chirality (see SM). The magnon dispersions are also gapped as depicted in Fig. 4 similar to the case without magnetic field. However, the gap excitations with and without the magnetic field are different which can be shown by solving for the chiral edge modes. The magnon edge modes for a strip geometry with open boundary conditions along the y -direction and infinite along x -direction are shown in Fig. 5 at zero magnetic field (top panel). We see that the system does not possess topologically protected gapless edge modes and the Chern number vanishes (see SM). On the other hand, the edge modes at finite magnetic field shown in bottom panel of Fig. 5 are gapless — an indication of a topological system. The magnetic-field-induced noncoplanar spin texture does not require a DM interaction in general as long-range order can be induced through other interactions. Besides, the scalar spin chirality χ_{ijk} should have the same effects on magnetic excitations in the CSL.

V. TOPOLOGICAL THERMAL HALL EFFECT

The existing conjecture is that the thermal Hall effect is present in the pure QKAF due to a Lorentz force in the deconfined fermionic spinons coupled to an emergent gauge field [38]. However, the charge-neutral magnetic excitations should not feel a Lorentz force and the

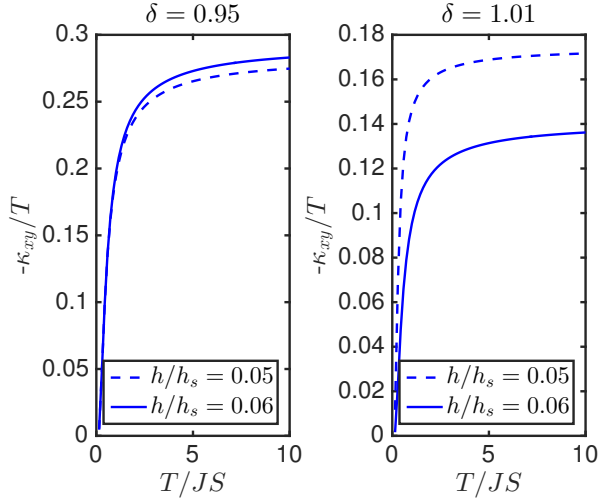


FIG. 6. Color online. Low temperature dependence of the topological thermal Hall conductivity with $D_{\perp}/J = 0.2$.

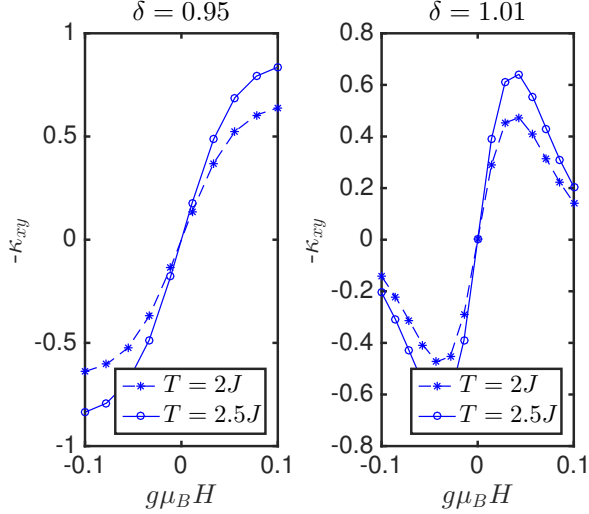


FIG. 7. Color online. Field dependence of the topological thermal Hall conductivity at low temperatures with $D_{\perp}/J = 0.2$.

DM interaction and external magnetic field have a profound effect on frustrated magnets which were not taken into account. Therefore the mechanism that gives rise to a nonzero thermal Hall effect in insulating frustrated magnets remains an open question until now. In the topological Hall effect an unconventional Hall conductivity is induced by the scalar spin chirality resulting from the configuration of the spin textures rather than the spin-orbit interaction as reported in several electronic (metallic) systems [70–73]. In the present model the magnetic excitations are charge-neutral quasiparticles on the frustrated QKAF and the transverse Hall conductivity requires the presence of a temperature gradient $-\nabla T$ which induces a heat current \mathcal{J}^Q . From linear response theory, one obtains $\mathcal{J}_{\alpha}^Q = -\sum_{\beta} \kappa_{\alpha\beta} \nabla_{\beta} T$, where $\kappa_{\alpha\beta}$

is the thermal conductivity and the transverse component κ_{xy} is associated with the thermal Hall conductivity given explicitly in Ref. [40].

As expected from the analyses given above, there is no χ_{ijk} at zero magnetic field and we find vanishing κ_{xy} despite distortion-induced gap magnon dispersion. This further confirms that the system is topologically trivial at zero field irrespective of the DM interaction. For finite magnetic field a nonzero scalar spin chirality is induced. Figure 6 shows the low temperature dependence of κ_{xy} (in units of k_B/\hbar) for two values of the lattice distortion and the magnetic field. The topological Hall conductivity captures a negative value in both regimes $\delta < 1$ and $\delta > 1$. On the other hand, Fig. 7 shows the magnetic field dependence of κ_{xy} which shows a symmetric sign reversal as the magnetic field changes sign.

We also note that a second-nearest neighbour antiferromagnetic interaction or magnon-phonon interaction may be present in real materials, which will probably enhance the thermal Hall conductivity. However, finite thermal Hall conductivity still originates from nonzero χ_{ijk} . As noted above the DM interaction can be zero without affecting the thermal Hall conductivity as the second-nearest neighbour antiferromagnetic interaction or an easy-plane anisotropy also stabilizes the coplanar/noncollinear Néel order. Therefore, kagomé antiferromagnetic materials with a weak (negligible) DM interaction can possess a thermal Hall conductivity from the real space Berry curvature of the spin texture, which extends to CSL phases. We note that the role of magnetic field in the QKAF is different triplon bands in a dimerized quantum magnet [74], where no scalar spin chirality was induced $\chi_{ijk} = 0$. Therefore, topological magnetic excitations and thermal Hall effect stem from the DM interaction [74].

VI. CONCLUSION

In summary, we have studied topological magnetic excitations and thermal Hall effect induced by the real space Berry curvature of the spin texture on the distorted kagomé antiferromagnets applicable to vesignieite, edwardsite, and volborthite. The lack of inversion symmetry on the kagomé lattice allows a Dzyaloshinskii-Moriya (DM) interaction, which lifts the classical degeneracy and stabilizes the coplanar/noncollinear magnetic spin structure. We showed that although the distortion and DM interaction introduce gap magnetic excitations, the system remains topologically trivial with neither protected edge modes nor finite thermal Hall conductivity. By turning on an out-of-plane external magnetic field, we showed that a finite scalar spin chirality is induced from the topology of the spin configurations. This gives rise to a Berry curvature independent of the DM interaction. The topological real space Berry curvature persists in the chiral spin liquid (CSL) phase due to the presence of the scalar spin chirality.

For a frustrated one-dimensional (1D) spin chain the DM interaction can be removed by a gauge transformation [75]. Most importantly, an ideal 1D system should not have a chiral noncoplanar magnetic order and scalar spin chirality should be absent. This suggests that the experimental result of thermal Hall response in volborthite can be best described using a distorted Heisenberg model as opposed to a frustrated alternating spin chain. An alternative approach is the Schwinger boson formalism, however in this formalism the scalar spin chirality does not appear explicitly on the kagomé antiferromagnets. Instead the DM interaction generates a magnetic flux leading to topological spin excitations even in the absence of an applied magnetic field [43, 76]. This is reminiscent of collinear ferromagnets and thus sharply contrast with the present results.

Our results call for further investigation of thermal Hall effect in the kagomé volborthite and other distorted quantum kagomé antiferromagnets such as vesignieite [17–23] and edwardsite [24]. Although we captured a negative thermal Hall conductivity (κ_{xy}) as seen in experiment [57], it would be interesting to determine the pa-

rameter values of volborthite and also measure the magnetic field dependence of κ_{xy} and possibly the topological magnetic excitations at various magnetic field and temperature ranges. Furthermore, experiment should also try to measure the spontaneous or magnetic-field-induced scalar spin chirality that gives rise to topological magnetic excitations and thermal Hall response. We believe that the results of this paper have shed some light on recent observation of thermal Hall conductivity in volborthite [57].

ACKNOWLEDGMENTS

The author would like to thank M. Yamashita, for elaborating on the experimental result of thermal Hall response in kagomé volborthite. Research at Perimeter Institute is supported by the Government of Canada through Industry Canada and by the Province of Ontario through the Ministry of Research and Innovation.

-
- [1] V. Kalmeyer and R. B. Laughlin, Phys. Rev. Lett. **59**, 2095 (1987).
 - [2] X. G. Wen, Frank Wilczek, and A. Zee, Phys. Rev. B **39**, 11413 (1989).
 - [3] G. Baskaran, Phys. Rev. Lett. **63**, 2524 (1989).
 - [4] B. Bauer, L. Cincio, B. P. Keller, M. Dolfi, G. Vidal, S. Trebst, A. W. W. Ludwig, Nature Communications **5**, 5137 (2014).
 - [5] Shou-Shu Gong, Wei Zhu, Leon Balents, and D. N. Sheng, Phys. Rev. B **91**, 075112 (2015).
 - [6] Alexander Wietek, Antoine Sterdyniak, and Andreas M. Läuchli Phys. Rev. B **92**, 125122 (2015).
 - [7] Samuel Bieri, Laura Messio, Bernard Bernu, and Claire Lhuillier, Phys. Rev. B **92**, 060407(R) (2015).
 - [8] S.-S. Gong, W. Zhu, and D.N. Sheng, Sci. Rep. **4**, 6317 (2014).
 - [9] J.-C. Domenge, P. Sindzingre, C. Lhuillier, and L. Pierre, Phys. Rev. B **72**, 024433 (2005).
 - [10] Yin-Chen He, D. N. Sheng, Yan Chen, Phys. Rev. Lett. **112**, 137202 (2014).
 - [11] I. Dzyaloshinsky, J. Phys. Chem. Solids **4**, 241 (1958).
 - [12] T. Moriya, Phys. Rev. **120**, 91 (1960).
 - [13] M. Elhajal, B. Canals, and C. Lacroix, Phys. Rev. B **66**, 014422 (2002).
 - [14] Daniel Grohol, Daniel G. Nocera, and Dimitris Papoutsakis, Phys. Rev. B **67**, 064401 (2003).
 - [15] D. Grohol, K. Matan, J.H. Cho, S.-H. Lee, J.W. Lynn, D.G. Nocera, Y.S. Lee, Nature Materials **4**, 323 (2005).
 - [16] K. Matan, D. Grohol, D. G. Nocera, T. Yildirim, A. B. Harris, S. H. Lee, S. E. Nagler, and Y. S. Lee, Phys. Rev. Lett. **96**, 247201 (2006).
 - [17] Y. Okamoto, H. Yoshida, and Z. Hiroi, J. Phys. Soc. Jpn. **78**, 033701 (2009).
 - [18] R. H. Colman, F. Bert, D. Boldrin, A. D. Hillier, P. Manuel, P. Mendels, and A. S. Wills, Phys. Rev. B **83**, 180416(R) (2011).
 - [19] J. A. Quilliam, F. Bert, R. H. Colman, D. Boldrin, A. S. Wills, and P. Mendels Phys. Rev. B **84**, 180401(R) (2011).
 - [20] M. Yoshida, Y. Okamoto, M. Takigawa, and Z. Hiroi, J. Phys. Soc. Jpn. **82**, 013702 (2013).
 - [21] H. Yoshida, Y. Michiue, E. Takayama-Muromachi, and M. Isobe, J. Mater. Chem. **22** 18793 (2012).
 - [22] H. Yoshida, Y. Michiue, E. Takayama-Muromachi, and M. Isobe, J. Mater. Chem. **22**, 18793 (2012).
 - [23] A. Zorko, F. Bert, A. Ozarowski, J. van Tol, D. Boldrin, A. S. Wills, and P. Mendels, Phys. Rev. B **88**, 144419 (2013).
 - [24] Hajime Ishikawa, Yoshihiko Okamoto, and Zenji Hiroi, J. Phys. Soc. Jpn. **82**, 063710 (2013).
 - [25] Z. Hiroi, M. Hanawa, N. Kobayashi, M. Nohara, H. Takagi, Y. Kato and M. Takigawa, J. Phys. Soc. Jpn. **70**, 3377 (2001).
 - [26] M. Yoshida, M. Takigawa, H. Yoshida, Y. Okamoto, and Z. Hiroi, Phys. Rev. Lett. **103**, 077207 (2009).
 - [27] M. Yoshida, M. Takigawa, S. Kramer, S. Mukhopadhyay, M. Horvatic, C. Berthier, H. Yoshida, Y. Okamoto, Z. Hiroi, J. Phys. Soc. Jpn. **81**, 024703 (2012).
 - [28] H. Ishikawa, M. Yoshida, K. Nawa, M. Jeong, S. Krämer, M. Horvatic, C. Berthier, M. Takigawa, M. Akaki, A. Miyake, M. Tokunaga, K. Kindo, J. Yamaura, Y. Okamoto, Z. Hiroi, Phys. Rev. Lett. **114**, 227202 (2015).
 - [29] M. R. Norman, Rev. Mod. Phys. **88**, 041002 (2016).
 - [30] A. Zorko, S. Nellutla, J. van Tol, L. C. Brunel, F. Bert, F. Duc, J.-C. Trombe, M. A. de Vries, A. Harrison, and P. Mendels, Phys. Rev. Lett. **101**, 026405 (2008).
 - [31] C. Balz, B. Lake, J. Reuther, H. Luetkens, R. Schönmann, Th. Herrmannsdörfer, Y. Singh, A.T.M. Nazmul Islam, E. M. Wheeler, J. A. Rodriguez-Rivera, T. Guidi, G. G. Simeoni, C. Baines, and H. Ryll, Nature Phys. **12**,

- 942 (2016).
- [32] T. -H. Han, J. S. Helton, S. Chu, D. G. Nocera, J. A. Rodriguez-Rivera, C. Broholm, Y. S. Lee, *Nature* **492**, 406 (2012).
 - [33] M. Jeong, F. Bert, P. Mendels, F. Duc, J. C. Trombe, M. A. de Vries, and A. Harrison, *Phys. Rev. Lett.* **107**, 237201 (2011).
 - [34] D. P. Kozlenko, A. F. Kusmartseva, E. V. Lukin, D. A. Keen, W. G. Marshall, M. A. de Vries, and K. V. Kamenev, *Phys. Rev. Lett.* **108**, 187207 (2012).
 - [35] Max Hirschberger, Robin Chisnell, Young S. Lee, and N. P. Ong, *Phys. Rev. Lett.* **115**, 106603 (2015).
 - [36] Y. Onose, T. Ideue, H. Katsura, Y. Shiomi, N. Nagaosa, Y. Tokura, *Science* **329**, 297 (2010).
 - [37] T. Ideue, Y. Onose, H. Katsura, Y. Shiomi, S. Ishiwata, N. Nagaosa, and Y. Tokura, *Phys. Rev. B* **85**, 134411 (2012).
 - [38] H. Katsura, N. Nagaosa, and P. A. Lee, *Phys. Rev. Lett.* **104**, 066403 (2010).
 - [39] R. Matsumoto and S. Murakami, *Phys. Rev. Lett.* **106**, 197202 (2011); *Phys. Rev. B* **84**, 184406 (2011).
 - [40] R. Matsumoto, R. Shindou, and S. Murakami, *Phys. Rev. B* **89**, 054420 (2014).
 - [41] L. Zhang, J. Ren, J. S. Wang, and B. Li, *Phys. Rev. B* **87**, 144101 (2013).
 - [42] A. Mook, J. Henk, and I. Mertig, *Phys. Rev. B* **90**, 024412 (2014); A. Mook, J. Henk, and I. Mertig, *Phys. Rev. B* **89**, 134409 (2014).
 - [43] H. Lee, J. H. Han, and P. A. Lee, *Phys. Rev. B* **91**, 125413 (2015).
 - [44] R. Chisnell, J. S. Helton, D. E. Freedman, D. K. Singh, R. I. Bewley, D. G. Nocera, and Y. S. Lee, *Phys. Rev. Lett.* **115**, 147201 (2015).
 - [45] A. L. Chernyshev and P. A. Maksimov, *Phys. Rev. Lett.* **117**, 187203 (2016).
 - [46] Jung Hoon Han and Hyunyoung Lee, *J. Phys. Soc. Jpn.* **86**, 011007 (2017).
 - [47] S. A. Owerre, *J. Phys.: Condens. Matter* **28**, 386001 (2016).
 - [48] S. A. Owerre, *J. Appl. Phys.* **120**, 043903 (2016).
 - [49] Se Kwon Kim, Héctor Ochoa, Ricardo Zarzuela, Yaroslav Tserkovnyak, *Phys. Rev. Lett.* **117**, 227201 (2016).
 - [50] Mook, A., Henk, J. and Mertig, *Phys. Rev. Lett.*, **117**, 157204 (2016).
 - [51] Y. Su, X. S. Wang, X. R. Wang, *arXiv:1609.01500* (2016).
 - [52] M. Z. Hasan and C. L. Kane, *Rev. Mod. Phys.* **82**, 3045 (2010).
 - [53] X.-L. Qi and S.-C. Zhang, *Rev. Mod. Phys.* **83**, 1057 (2011).
 - [54] Xiangang Wan, Ari M. Turner, Ashvin Vishwanath, and Sergey Y. Savrasov, *Phys. Rev. B* **83**, 205101 (2011).
 - [55] A. A. Burkov and L. Balents, *Phys. Rev. Lett.* **107**, 127205 (2011).
 - [56] S. A. Owerre, *J. Phys.: Condens. Matter* **28**, 235501 (2016).
 - [57] D. Watanabe, K. Sugii, M. Shimozaawa, Y. Suzuki, T. Yajima, H. Ishikawa, Z. Hiroi, T. Shibauchi, Y. Matsuda, M. Yamashita, *Proc. Natl. Acad. Sci. USA* **113**, 8653 (2016).
 - [58] M. Yamashita, Private Communication.
 - [59] O. Cépas, C. M. Fong, P. W. Leung, and C. Lhuillier *Phys. Rev. B* **78**, 140405(R) (2008).
 - [60] Andreas P. Schnyder, Oleg A. Starykh, and Leon Balents *Phys. Rev. B* **78**, 174420 (2008).
 - [61] O. Janson, J. Richter, P. Sindzingre, H. Rosner, *Phys. Rev. B* **82**, 104434 (2010).
 - [62] O. Janson, S. Furukawa, T. Momoi, P. Sindzingre, J. Richter, K. Held, *Phys. Rev. Lett.* **117**, 037206 (2016).
 - [63] W. Apel, T. Yavors'kii, H.-U. Everts, *J. Phys.: Condens. Matter* **19**, 145255 (2007).
 - [64] P. Sindzingre, *arXiv:0707.4264*.
 - [65] Fa Wang, Ashvin Vishwanath, and Yong Baek Kim, *Phys. Rev. B* **76**, 094421 (2007).
 - [66] P. H. Y. Li, R. F. Bishop, C. E. Campbell, D. J. J. Farnell, O. Götze, and J. Richter, *Phys. Rev. B* **86**, 214403 (2012).
 - [67] Edward Parker and Leon Balents, *arXiv:1610.03135* (2016).
 - [68] T. Holstein and H. Primakoff, *Phys. Rev.* **58**, 1098 (1940).
 - [69] A. Scheie, M. Sanders, J. Krizan, Y. Qiu, R.J. Cava, C. Broholm, *Phys. Rev. B* **93**, 180407 (2016).
 - [70] Y. Taguchi, Y. Oohara, H. Yoshizawa, N. Nagaosa, Y. Tokura, *Science* **291**, 2573 (2001).
 - [71] Y. Machida, S. Nakatsuji, Y. Maeno, T. Tayama, T. Sakakibara, and S. Onoda, *Phys. Rev. Lett.* **98**, 057203 (2007).
 - [72] Y. Machida, S. Nakatsuji, S. Onoda, T. Tayama, and T. Sakakibara, *Nature*, **463**, 210 (2008).
 - [73] Jian Zhou, Qi-Feng Liang, Hongming Weng, Y. B. Chen, Shu-Hua Yao, Yan-Feng Chen, Jinming Dong, and Guang-Yu Guo, *Phys. Rev. Lett.* **116**, 256601 (2016).
 - [74] Judit Romhányi, Karlo Penc, R. Ganesh, *Nature Communications* **6**, 6805 (2015).
 - [75] Vladimir A. Zyuzin and Gregory A. Fiete, *Phys. Rev. B* **85**, 104417 (2012).
 - [76] L. Messio, O. Cépas, and C. Lhuillier, *Phys. Rev. B* **81**, 064428 (2010).

Topological Magnetic Excitations on the Distorted Kagomé Antiferromagnets Supplemental Material

S. A. Owerre^{1,2}

¹*Perimeter Institute for Theoretical Physics, 31 Caroline St. N., Waterloo, Ontario N2L 2Y5, Canada.*

²*African Institute for Mathematical Sciences, 6 Melrose Road, Muizenberg, Cape Town 7945, South Africa.*

(Dated: December 3, 2024)

I. MODEL HAMILTONIAN

We consider the Hamiltonian for kagomé antiferromagnets with DM interaction and Zeeman magnetic field given by

$$\mathcal{H} = \sum_{\langle i,j \rangle} [J_{ij} \mathbf{S}_i \cdot \mathbf{S}_j + \mathbf{D}_{ij} \cdot \mathbf{S}_i \times \mathbf{S}_j] - \mathbf{H} \cdot \sum_i \mathbf{S}_i, \quad (1)$$

where $\mathbf{H} = h\hat{\mathbf{z}}$, $h = g\mu_B H$ and $\mathbf{D}_{ij} = -D_\perp \hat{\mathbf{z}}$. This particular case of out-of-plane DM interaction is very common in most distorted kagomé antiferromagnetic materials. It is also interesting because topological magnetic excitations are not induced by the DM interaction as we will show. The presence of out-of-plane DM interactions breaks the complete SU(2) rotation symmetry down to U(1) symmetry about the z -axis. The classical energy is given by

$$e_0(\phi) = 2J(2 + \delta) [(1 - \cos \vartheta) \cos^2 \phi + \cos \vartheta] - 4D_\perp \sin^2 \phi \sin \vartheta (1 - \cos \vartheta) - 3h \cos \phi, \quad (2)$$

where $e_0(\phi) = E(\phi)/NS^2$, N is the number of sites per unit cell, and $\vartheta = \arccos(-1/2\delta)$ which is not exactly 120° for $\delta \neq 1$. The magnetic field is rescaled in unit of S . The minimization of $e_0(\phi)$ yields the field-induced canting angle $\cos \phi = h/h_s$ where

$$h_s = \frac{(1 - \cos \vartheta)}{3} [4J(2 + \delta) + 8D_\perp \sin \vartheta]. \quad (3)$$

The excitations above the classical ground state are obtained as follows. The procedure involves performing a rotation about the z -axis on the triad by the spin oriented angles ϑ in order to achieve the coplanar configuration. As the out-of-plane magnetic field is turned on, we have to align the spins along the new quantization axis by performing a rotation about the y -axis by the field canting angle ϕ . The total rotation matrix takes the form

$$\mathbf{S}_i = \mathcal{R}_z(\theta_i) \cdot \mathcal{R}_y(\phi) \cdot \mathbf{S}'_i, \quad (4)$$

where

$$\mathcal{R}_z(\theta_i) \cdot \mathcal{R}_y(\phi) = \begin{pmatrix} \cos \theta_i \cos \phi & -\sin \theta_i & \cos \theta_i \sin \phi \\ \sin \theta_i \cos \phi & \cos \theta_i & \sin \theta_i \sin \phi \\ -\sin \phi & 0 & \cos \phi \end{pmatrix}, \quad (5)$$

and $\theta_i = \vartheta_{A,B,C}$. In the following, we drop the prime in the rotated coordinate. At low temperatures accessible

experimentally, the noninteracting magnon model sufficiently describes the system. The corresponding Hamiltonian that contribute to noninteracting magnon model is given by

$$\mathcal{H}_J = \sum_{\langle i,j \rangle} J_{ij} [\cos \theta_{ij} \mathbf{S}_i \cdot \mathbf{S}_j + \sin \theta_{ij} \cos \phi \hat{\mathbf{z}} \cdot (\mathbf{S}_i \times \mathbf{S}_j)] \quad (6)$$

$$+ 2 \sin^2 \left(\frac{\theta_{ij}}{2} \right) (\sin^2 \phi S_i^x S_j^x + \cos^2 \phi S_i^z S_j^z),$$

$$\mathcal{H}_{DM} = D_\perp \sum_{\langle i,j \rangle} [\sin \theta_{ij} (\cos^2 \phi S_i^x S_j^x + S_i^y S_j^y) \quad (7)$$

$$+ \sin^2 \phi S_i^z S_j^z] - \cos \theta_{ij} \cos \phi \hat{\mathbf{z}} \cdot (\mathbf{S}_i \times \mathbf{S}_j),$$

$$\mathcal{H}_h = -h \cos \phi \sum_i S_i^z, \quad (8)$$

where $\theta_{ij} = \theta_i - \theta_j$. At zero magnetic field, i.e., $\phi = \pi/2$, the chiral interaction is absent in the magnon model despite the the presence of DM interaction. Hence, the system is topologically trivial at zero field. The magnetic-field-induced scalar spin chirality

$$\mathcal{H}_\chi = \sum_{i,j,k=\Delta} \chi_{ijk}, \quad (9)$$

originates from noncoplanar spin texture formed by the spin triad $\mathbf{S}_i, \mathbf{S}_j, \mathbf{S}_k$, where $\chi_{ijk} = \mathbf{S}_i \cdot (\mathbf{S}_j \times \mathbf{S}_k)$. It is well-known that $\langle \chi_{ijk} \rangle$ can be nonzero even in the absence of magnetic ordering $\langle \mathbf{S}_j \rangle = 0$, e.g. in chiral spin liquid phase. This is a very crucial difference between collinear ferromagnets and antiferromagnets on the kagomé lattice. To obtain the magnon dispersions, we proceed as usual by introducing the Holstein Primakoff spin bosonic operators

$$S_i^z = S - a_i^\dagger a_i, \quad (10)$$

$$S_i^y = i\sqrt{\frac{S}{2}}(a_i^\dagger - a_i), \quad (11)$$

$$S_i^x = \sqrt{\frac{S}{2}}(a_i^\dagger + a_i), \quad (12)$$

where $a_i^\dagger(a_i)$ are the bosonic creation (annihilation) operators. The noninteracting magnon tight binding Hamil-

tonian is given by

$$\begin{aligned} \mathcal{H} = S \sum_{\langle i,j \rangle} [G_{ij}^z(a_i^\dagger a_i + a_j^\dagger a_j) + G_{ij}^d(e^{-i\Phi_{ij}} a_i^\dagger a_j + h.c.)] \\ + G_{ij}^o(a_i^\dagger a_j^\dagger + h.c.)] + h_\phi \sum_i a_i^\dagger a_i, \end{aligned} \quad (13)$$

where

$$G_{ij}^z = -J_{ij}[\cos \theta_{ij} + 2 \cos^2 \phi \sin^2(\theta_{ij}/2)] - \mathcal{D}_\perp \sin^2 \phi \sin \theta_{ij}, \quad (14)$$

$$G_{ij}^d = \sqrt{(G_{ij}^R)^2 + (G_{ij}^M)^2}, \quad (15)$$

$$G_{ij}^R = J_{ij} \left[\cos \theta_{ij} + \frac{2 \sin^2 \phi \sin^2(\theta_{ij}/2)}{2} \right] + D_\perp \sin \theta_{ij} \left(1 - \frac{\sin^2 \phi}{2} \right), \quad (16)$$

$$G_{ij}^M = \cos \phi (J_{ij} \sin \theta_{ij} - D_\perp \cos \theta_{ij}), \quad (17)$$

$$G_{ij}^o = \frac{\sin^2 \phi}{2} (2J_{ij} \sin^2(\theta_{ij}/2) - D_\perp \sin \theta_{ij}), \quad (18)$$

and $h_\phi = h \cos \phi$. The fictitious magnetic flux or solid angle subtended by three noncoplanar spins is given by $\tan \Phi_{ij} = G_{ij}^M / G_{ij}^R$. We clearly see that Φ_{ij} is nonzero in the absence of DM interaction. It should be noted that the $\mathbf{Q} = \mathbf{0}$ magnetic structure that can be stabilized by other means as mentioned in the text. In momentum space we obtain

$$\begin{aligned} \mathcal{H} = S \sum_{\mathbf{k}, \alpha, \beta} (2\mathcal{M}_{\alpha\beta}^z \delta_{\alpha\beta} + 2\mathcal{M}_{\alpha\beta}^d) a_{\mathbf{k}\alpha}^\dagger a_{\mathbf{k}\beta} \\ + \mathcal{M}_{\alpha\beta}^o (a_{\mathbf{k}\alpha}^\dagger a_{-\mathbf{k}\beta}^\dagger + a_{\mathbf{k}\alpha} a_{-\mathbf{k}\beta}), \end{aligned} \quad (19)$$

where $\alpha, \beta = A, B, C$ and the coefficients are given by

$$\mathcal{M}^z = \text{diag}(\zeta_{AA}, \zeta_{BB}, \zeta_{CC}), \quad (20)$$

with $\zeta_{AA} = G_{AB}^z + G_{CA}^z + h_\phi/2$, $\zeta_{BB} = \zeta_{CC} = G_{AB}^z + G_{BC}^z + h_\phi/2$.

$$\mathcal{M}^d = \begin{pmatrix} 0 & \gamma_{AB}^d e^{-i\Phi_{AB}} & \gamma_{CA}^d e^{i\Phi_{CA}} \\ \gamma_{AB}^{*d} e^{i\Phi_{AB}} & 0 & \gamma_{BC}^d e^{-i\Phi_{BC}} \\ \gamma_{CA}^{*d} e^{-i\Phi_{CA}} & \gamma_{BC}^{*d} e^{i\Phi_{BC}} & 0 \end{pmatrix}, \quad (21)$$

$$\mathcal{M}^o = \begin{pmatrix} 0 & \gamma_{AB}^o & \gamma_{CA}^o \\ \gamma_{AB}^{*o} & 0 & \gamma_{BC}^o \\ \gamma_{CA}^{*o} & \gamma_{BC}^{*o} & 0 \end{pmatrix}, \quad (22)$$

where $\gamma_{AB}^d = G_{AB}^d \cos k_1$, $\gamma_{BC}^d = G_{BC}^d \cos k_2$, $\gamma_{CA}^d = G_{CA}^d \cos k_3$; $\gamma_{AB}^o = G_{AB}^o \cos k_1$, $\gamma_{BC}^o = G_{BC}^o \cos k_2$, $\gamma_{CA}^o = G_{CA}^o \cos k_3$. $k_i = \mathbf{k}_i \cdot \mathbf{e}_i$, and $\mathbf{e}_1 = (-1/2, -\sqrt{3}/2)$, $\mathbf{e}_2 = (1, 0)$, $\mathbf{e}_3 = (-1/2, \sqrt{3}/2)$. The Hamiltonian can be written as

$$\mathcal{H} = S \sum_{\mathbf{k}} \Psi_{\mathbf{k}}^\dagger \mathcal{H}(\mathbf{k}) \Psi_{\mathbf{k}} - \text{const.}, \quad (23)$$

where $\Psi_{\mathbf{k}}^\dagger = (b_{\mathbf{k}A}^\dagger, b_{\mathbf{k}B}^\dagger, b_{\mathbf{k}C}^\dagger, b_{-\mathbf{k}A}, b_{-\mathbf{k}B}, b_{-\mathbf{k}C})$, and

$$\mathcal{H}(\mathbf{k}) = \begin{pmatrix} \mathcal{M}^z + \mathcal{M}^d & \mathcal{M}^o \\ \mathcal{M}^o & \mathcal{M}^z + \mathcal{M}^d \end{pmatrix}. \quad (24)$$

In the undistorted limit $\delta \rightarrow 1$, $\zeta_{AA} = \zeta_{BC} = \zeta_{CA}$. The resulting magnon bands at zero field $\mathcal{H}_\chi = 0$ has a flat constant mode. For the distorted case $\delta \neq 1$ the situation is different. We have $\zeta_{AA} > \zeta_{BC}$, ζ_{CA} for $\delta < 1$ and $\zeta_{AA} < \zeta_{BC}$, ζ_{CA} for $\delta > 1$. The magnon bands at zero field $\mathcal{H}_\chi = 0$ no longer have a flat constant mode in the entire Brillouin zone see main text.

II. MATRIX DIAGONALIZATION

The Hamiltonian is diagonalized by the generalized Bogoliubov transformation $\Psi_{\mathbf{k}} = \mathcal{P}_{\mathbf{k}} Q_{\mathbf{k}}$, where $\mathcal{P}_{\mathbf{k}}$ is a $2N \times 2N$ paraunitary matrix and $Q_{\mathbf{k}}^\dagger = (Q_{\mathbf{k}}^\dagger, Q_{-\mathbf{k}}^\dagger)$ with $Q_{\mathbf{k}}^\dagger = (\beta_{\mathbf{k}A}^\dagger, \beta_{\mathbf{k}B}^\dagger, \beta_{\mathbf{k}C}^\dagger)$ being the quasiparticle operators. The matrix $\mathcal{P}_{\mathbf{k}}$ satisfies the relations,

$$\mathcal{P}_{\mathbf{k}}^\dagger \mathcal{H}(\mathbf{k}) \mathcal{P}_{\mathbf{k}} = \mathcal{E}_{\mathbf{k}} \quad (25)$$

$$\mathcal{P}_{\mathbf{k}}^\dagger \tau_3 \mathcal{P}_{\mathbf{k}} = \tau_3, \quad (26)$$

where $\mathcal{E}_{\mathbf{k}} = \text{diag}(\omega_{\mathbf{k}\alpha}, \omega_{-\mathbf{k}\alpha})$, $\tau_3 = \text{diag}(\mathbf{I}_{N \times N}, -\mathbf{I}_{N \times N})$, and $\omega_{\mathbf{k}\alpha}$ are the energy eigenvalues. From Eq. 26 we get $\mathcal{P}_{\mathbf{k}}^\dagger = \tau_3 \mathcal{P}_{\mathbf{k}}^{-1} \tau_3$, and Eq. 25 is equivalent to saying that we need to diagonalize the Hamiltonian $\mathcal{H}'(\mathbf{k}) = \tau_3 \mathcal{H}(\mathbf{k})$, whose eigenvalues are given by $\tau_3 \mathcal{E}_{\mathbf{k}}$ and the columns of $\mathcal{P}_{\mathbf{k}}$ are the corresponding eigenvectors. The eigenvalues of this Hamiltonian cannot be obtained analytically except at zero field. The paraunitary operator $\mathcal{P}_{\mathbf{k}}$ defines a Berry curvature given by

$$\Omega_{ij;\alpha}(\mathbf{k}) = -2\text{Im}[\tau_3(\partial_{k_i} \mathcal{P}_{\mathbf{k}\alpha}^\dagger) \tau_3(\partial_{k_j} \mathcal{P}_{\mathbf{k}\alpha})]_{\alpha\alpha}, \quad (27)$$

with $i, j = \{x, y\}$ and $\mathcal{P}_{\mathbf{k}\alpha}$ are the columns of $\mathcal{P}_{\mathbf{k}}$. In this form, the Berry curvature simply extracts the diagonal components which are the most important. From Eq. 25 the Berry curvature can be written alternatively as

$$\Omega_{ij;\alpha}(\mathbf{k}) = -2 \sum_{\alpha' \neq \alpha} \frac{\text{Im}[\langle \mathcal{P}_{\mathbf{k}\alpha} | v_i | \mathcal{P}_{\mathbf{k}\alpha'} \rangle \langle \mathcal{P}_{\mathbf{k}\alpha'} | v_j | \mathcal{P}_{\mathbf{k}\alpha} \rangle]}{(\omega_{\mathbf{k}\alpha} - \omega_{\mathbf{k}\alpha'})^2}, \quad (28)$$

where $\mathbf{v} = \partial \mathcal{H}'(\mathbf{k}) / \partial \mathbf{k}$ defines the velocity operators. The Berry curvature is related to the solid angle $\Omega(\mathbf{k}) \propto \Phi$ and the Chern number is defined as,

$$\mathcal{C}_\alpha = \frac{1}{2\pi} \int_{BZ} dk_x dk_y \Omega_{xy;\alpha}(\mathbf{k}). \quad (29)$$

It can be shown that the Chern numbers are related to the scalar-chirality-induced fictitious flux Φ as $\mathcal{C}_1 = 0$, $\mathcal{C}_2 = -\text{sgn}(\sin(\Phi))$, $\mathcal{C}_3 = \text{sgn}(\sin(\Phi))$, where

$$\sin(\Phi) = \frac{1}{2} \chi_{ijk}. \quad (30)$$